# Corrections to the usual x-ray scattering factors in rare gases: Experiment and theory

L. Young, R. W. Dunford, E. P. Kanter, B. Krässig, and S. H. Southworth
*Chemistry Division, Argonne National Laboratory, Argonne, Illinois 60439*

R. A. Bonham, P. Lykos, C. Morong, and A. Timm
*Department of Biological, Chemical, and Physical Sciences, Illinois Institute of Technology, Chicago, Illinois 60616*

J. P. J. Carney and R. H. Pratt
*Department of Physics and Astronomy, University of Pittsburgh, Pittsburgh, Pennsylvania 15260*
(Received 18 December 2000; published 18 April 2001)

The ratio of the total x-ray scattering from Ne to that from He has been determined for photon energies in the range 4–15 keV at scattering angles of 45 and 90 degrees (corresponding to momentum transfers ranging from 0.90 to 5.69 a.u.). An arrangement of two gas cells in series was employed, allowing simultaneous measurements on both gases at the same scattering angle, which eliminates possible errors due to fluctuating beam intensity. Pairs of measurements corresponding to the same momentum transfer (at momentum transfers of 1.67 and 3.08 a.u.) but to different energies, provide a direct test of the corrections to the (momentum-transfer-dependent) form-factor incoherent-scattering-factor theory. These corrections include the anomalous $\boldsymbol{p}\cdot\boldsymbol{A}$ contributions, which are found to be important. We also consider corrections to the usual approximations made within the inelastic $A^2$ theory (the incoherent-scattering factor, using closure approximation, and the impulse approximation, assuming free-particle kinematics with a given momentum distribution). In these cases an incoherent-scattering-factor treatment is generally adequate, while anomalous scattering factor corrections to form factors are needed for elastic scattering.

DOI: 10.1103/PhysRevA.63.052718 PACS number(s): 32.80.Cy

## I. INTRODUCTION

We report precision measurements of x-ray scattering from He and Ne gas targets, obtaining agreement between theory and experiment only after performing a detailed theoretical analysis that goes beyond the current tabulations of elastic and inelastic photon-atom scattering cross sections. This paper follows in the path of two previous studies in which the experimental precision obtained stringently tested the available theoretical predictions of the day: (1) The study by Chipman and Jennings in 1963 [1] reported precisions of 0.5%, and at the time only the newest atomic structure calculations were of sufficient quality for agreement. (2) The study of Jung *et al.* in 1998 [2] was aided by the availability of high-intensity third-generation synchrotron sources, and while it covered a similar energy range to that of Ref. [1] much larger momentum transfers were involved, revealing the need for the inclusion of nonlocal exchange, electron correlation, and $\boldsymbol{p}\cdot\boldsymbol{A}$ contributions. Because the effects of target electron correlation and nonlocal exchange are well documented for both He and Ne [3–5], it was decided to extend the studies of Ref. [2] to lower energies, where the effects of the $\boldsymbol{p}\cdot\boldsymbol{A}$ terms in the nonrelativistic x-ray scattering theory are expected to be larger, and where commonly made approximations in the $A^2$ theory of inelastic scattering (incoherent scattering factor, impulse approximation) are more questionable.

One finds that different experiments and regimes tend to emphasize different effects (a quantitative discussion for the three experiments is given in Sec. III C). As mentioned in Ref. [2] and discussed extensively in Ref. [6], one does not in general have a single available theoretical approach that includes all the effects that may be important. There are no readily available tabulations of cross sections that give ratios of total scattering from Ne and from He that are in agreement with the present experiment. Below we outline a scheme for (in principle) obtaining the exact (nonrelativistic) result, and we identify two (approximate) implementations of that scheme (Methods A and B) which are compared with experiment in Sec. III. More details concerning these methods, their implementation, and the approximations they require, are given in Appendix A (see also Refs. [6,7]).

First, we assume that the scattering process is well-described nonrelativistically (with relativistic effects being included perturbatively, or else neglected entirely). The discussion for the nonrelativistic case will be in principle exact, with approximations appearing in the implementation only. We write the nonrelativistic photon-electron interaction Hamiltonian

$$H=-\frac{e}{mc}\boldsymbol{p}\cdot\boldsymbol{A}+\frac{e^2}{2mc^2}A^2, \tag{1}$$

and we consider the elastic- and inelastic-scattering processes. We will next assume that the contributions arising from the $\boldsymbol{p}\cdot\boldsymbol{A}$ terms can be adequately described using independent-particle-approximation results for both the elastic and inelastic processes. We find that the $\boldsymbol{p}\cdot\boldsymbol{A}$ contribution to inelastic scattering is insignificant, and one knows from photoeffect results (related to the forward elastic anomalous amplitudes through the optical theorem) that IPA results for the anomalous $\boldsymbol{p}\cdot\boldsymbol{A}$ contribution to elastic scattering are adequate [8], with beyond-IPA effects being significant in the $A^2$ form-factor contribution.

In elastic scattering the $A^2$ term gives rise to the form factor. Such form factors are widely available and are as good as the wave functions used. The $A^2$ term for inelastic

 

processes (Compton and Raman) requires more detailed discussion. Two well-known approximations are the incoherent-scattering-factor approximation (ISF) and the impulse approximation (IA). The ISF is an approximation employing closure and gives the total inelastic scattering (both Compton and Raman). The IA is an approximation to Compton only. Therefore using IA alone to describe the inelastic cross section corresponds to neglecting Raman entirely. In fact we find that one needs to include the (correlated $A^2$) Raman scattering cross section, since it is not generally insignificant in the total inelastic cross section, particularly for He where corrections of up to 5% are obtained.

Therefore one can either (a) take the ISF and add a correction to get the exact $A^2$ inelastic result, or (b) take IA and add a correction to get the exact $A^2$ Compton result, to which is then added the Raman $A^2$ result. Methods A and B (which are discussed in Appendix A) are approximate implementations of the procedures (a) and (b), respectively. Briefly Method A includes the leading terms in a series expansion of the needed correction to the ISF, based on sum rules that are satisfied by the generalized oscillator strength (GOS) that appears in the exact-$A^2$ inelastic cross section. Method B makes the assumption of considering corrections to the simplest calculation as linearly independent perturbations to the cross section, thus, for example, allowing the needed correction to IA to be estimated from uncorrelated exact-$A^2$ Compton calculations using local exchange. In Method B one then adds in the corresponding Raman $A^2$ result (which can be obtained using similar assumptions of linearly independent perturbations). More details on this, and references to the data used, are given in Appendix A. In both methods $\boldsymbol{p}\cdot\boldsymbol{A}$ corrections will then be added, as could relativistic corrections, if desired.

In the next section we describe the present experiment, with some further details in Appendices B and C. In Sec. III we compare the experimental results with various theoretical predictions, including those of the Methods A and B (which are described in more detail in Appendix A). Our conclusions are given in Sec. IV.

## II. EXPERIMENTAL DETAILS

### A. Data collection

The experiment was characterized by the use of two gas cells in series. A Si(Li) detector was mounted on the top of each cell at a scattering angle of 45° and another Si(Li) detector was on the bottom of each cell at a scattering angle of 90°. All four detectors were in a plane perpendicular to the plane of the synchrotron orbit, which contains the incident polarization vector. A schematic view of the apparatus is shown in Fig. 1. This arrangement allowed the simultaneous recording of x-rays scattered from Ne and He for each incident energy at both 45° and 90°. Each cell employed, 70-$\mu$m-thick Kapton windows for the side of the cell exposed to room pressure while 50-$\mu$m-thick Kapton windows were used at the ends of each cell facing the evacuated tube between cells. The exit windows on the paths leading to the detectors were 125-$\mu$m-thick Kapton. Additionally, the detector surfaces were covered by a 7.5-$\mu$m-thick Be film for

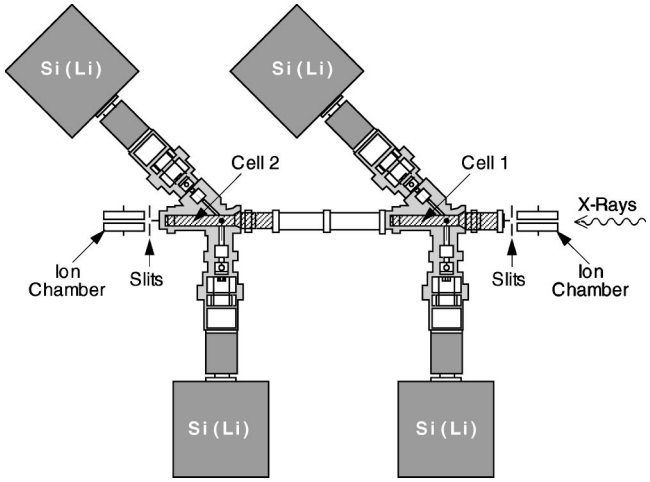


FIG. 1. Schematic illustration of the experimental apparatus.

both 45° detectors and by 25-$\mu$m-thick Be films for the two 90° detectors. The spaces between the two cells and between the exit windows for the scattered x-rays and the detectors were maintained at a pressure below 10 mtorr at all times. Ion chambers were placed in front of the first cell and behind the second with the space between the chambers and entrance and exit windows maintained at a He pressure slightly over 1 atm to reduce x-ray absorption. The experimental data were collected over a three day period on the BESSRC undulator beam line, 12-ID, at the Advanced Photon Source at Argonne National Laboratory. Available photon fluxes were approximately $10^{13}$ photons/s in a spot size of 1 mm$^2$ with an energy bandwidth of 0.01%. Aluminum attenuators were placed in the incident beam to produce count rates between 400 and 2000 counts/s. For all the experiments the beam current was externally stabilized to about 1%/h and was monitored by the ion chambers. The experimental arrangement employed here eliminated the need for deadtime, incident beam fluctuation, and ion chamber corrections required in an earlier study [2].

An experimental run consisted of filling the cell closest to the incoming beam (labeled cell 1) with about 1 atm of He and the second cell (labeled cell 2) with 20–40 torr of Ne and simultaneously recording the count rates of all four detectors for four to six consecutive 15 min data collection periods. The statistical uncertainty in the total number of counts accumulated was typically between 0.2 and 0.6%. The He pressure in cell 1 was monitored by a MKS Baratron 1000-torr absolute pressure gauge of $\pm 0.5\%$ reading accuracy (manufacturers specification) and the Ne pressure was monitored by a 100-torr gauge of the same type and accuracy. The two gauges were compared using He pressures between 20 and 100 torr and all Ne pressure measurements were corrected to the response of the 1000-torr gauge. Note that the cross section ratio determined in this experiment depends only on the ratio of the two pressures and not their absolute values.

A cell correction was determined by repeating the experiment with the two cells connected and filled to about 1 atm of He. The pressure in the combined cells was monitored with the 1000-torr gauge. In addition, background runs were

made at each energy with the cells evacuated in order to document x-ray fluorescence lines and scattering from gas cell walls and apertures. These data were used to subtract out background contributions from both the He-Ne and He-He runs.

### B. Data analysis

The two cells were machined as closely as possible to have identical dimensions. Assuming that absorption by windows of the same thickness is the same in the two cells then, within the machining accuracy, we can write for the intensities observed by two detectors at the same scattering angle

$$I_1(\theta,\hbar\omega_0)=I_0T_{w1}\exp[-(l_1+l_2)n_1\sigma_1]\Delta\Omega\Delta l n_1 \times\left(\frac{d\sigma_1^{\exp}(\theta,\hbar\omega_0)}{d\Omega}\right) \tag{2}$$

and

$$I_2(\theta,\hbar\omega_0)=I_0T_{w1}T_{w2}^2\exp[-(l_1+l_3)n_1\sigma_1-(l_1+l_2)n_2\sigma_2] \times\Delta\Omega\Delta l n_2\left(\frac{d\sigma_2^{\exp}(\theta,\hbar\omega_0)}{d\Omega}\right), \tag{3}$$

where $\theta,\hbar\omega_0$ specify the scattering angle and incident x-ray energy, $T_{w1},T_{w2}$ are the transmission factors for 70- and 50-$\mu$m-thick Kapton windows, respectively, $l_1,l_2$ are the distances from the cell entrance window to the beginning of the observable scattering region and from the observable scattering region to the detector window, respectively, $l_3=L-l_1$, where $L$ is the length of the cell, $n$ and $\sigma$ are the number density and total gas absorption cross section (photo absorption plus scattering) respectively, where the subscripts refer to the cell number, $\Delta\Omega$ is the solid acceptance angle of the detector, $\Delta l$ is the length of the incident x-ray beam visible to the detector, and $(d\sigma_{1,2}^{\exp}(\theta,\hbar\omega_0)/d\Omega)$ is given by

$$\left(\frac{d\sigma_{1,2}^{\exp}(\theta,\hbar\omega_0)}{d\Omega}\right)=\int_{E_{\min}}^{E_{\max}}dE\ T_{w3}(E)\int_{E_1}^{E_2}d\varepsilon\ R(E-\varepsilon) \times\left(\frac{d^2\sigma_{1,2}(\varepsilon)}{dEd\Omega}\right), \tag{4}$$

where the convolution integral over $\varepsilon$ of the product of the detector response, $R(\varepsilon)$, and the cross-section differential with respect to energy loss and detected solid angle, $d^2\sigma_2(\epsilon)/dEd\Omega$, is over the range $E_1$ to $E_2$, set by examining each spectrum. The limits for the remaining integral over the window transmission, $T_{w3}(E)$, through the 125 $\mu$m Kapton and Be films, $E_{\min}$ and $E_{\max}$, were determined for the numerical integration of the observed energy-loss spectrum so that the entire spectral width was included. These limits generally ranged from $-\hbar\omega_0$ to $+(3-4)$ keV in energy loss. The results were calculated with slightly different choices for the upper limit and the sensitivity to its choice was found to be less than 0.2%. A model analysis of the error incurred by assuming that $[d\sigma_{1,2}^{\exp}(\theta,\hbar\omega_0)/d\Omega]=\int_{E_{\min}}^{E_{\max}}dE\,[d^2\sigma_{1,2}(E)/dEd\Omega]$ is given in Appendix B, where it is pointed out that the most serious correction comes from the window transmission $T_{w3}(E)$. Corrections for the diminished registration of inelastic events relative to the elastic scattering have been applied to the experimental ratios.

It should be pointed out that the transmission $T_{w3}(E)$ through the window in front of the detector decreases with increasing energy loss, $E$, while the detector efficiency, $\xi(\alpha,E)$, increases, but only slightly, with increasing energy loss. The details are presented in Appendix B. Equation (C3), given in Appendix C, was used to correct the experimental ratios for gas and window absorption.

### C. Uncertainty estimates

The main error sources were the error in the pressure ratio, the error in the total number of counts accumulated, the error due to air contamination, and the uncertainty in the correction for gas absorption in the cell. The uncertainty in the pressure ratio was estimated by assuming the gauge manufacturers stated absolute uncertainty of $\pm0.5\%$ of the reading was the uncertainty in each of the two pressure measurements for a total estimate of $\pm0.71\%$ for the error in the pressure ratio. It is of interest to note that gauges are commercially available that are $\pm0.08\%$ in absolute accuracy but are also both $\pm0.01\%$ linear and reproducible, which means that with careful intergauge calibration, pressure errors in ratio measurements could probably be pushed to uncertainties as low as $\pm(0.02-0.04)\%$.

The error in the total number of counts accumulated in a 15 min collection period was taken as the square root of that total and when count totals were averaged over $n$ runs, the statistical uncertainty, $\Delta N_{\text{average}}$, was calculated as

$$\Delta N_{\text{average}}=\sqrt{\frac{\Sigma_{i=1}^{n}N_i}{n}}, \tag{5}$$

where $N_i$ is the total number of counts accumulated during the $i$th data collection segment. Typical values ranged from 0.3% on the low side to 0.7% on the high side.

Air contamination due to gas effusion through the Kapton windows appeared to mainly affect measurements made with He in a cell at pressures below 1 atm. Background corrections were applied to all the data runs and no He runs below atmospheric pressure were included in the analysis. No uncertainty estimate was made for possible error from this source except in the case of the 4.393 keV data, since it was the only energy for which clear evidence was available that air contamination was a serious problem.

The uncertainty in the gas absorption correction was estimated by assuming that the experimental pressure was uncertain by $\pm0.5\%$ and that all cell dimensions were uncertain by $\pm0.1$ cm. The tabular transmission values were assumed to be errorless. The gas absorption correction was appreciable only for the 4.393 keV data where the total correction was $17-18\%$.

A number of decisions had to be made in the data analysis that required judgment on the part of the observer. These included assigning the limits to the region of the spectrum containing double pulses, background subtraction, the width of the spectral region, and subtraction of fluorescent peaks. The uncertainty introduced as a result of these decision making processes was determined by three totally independent

TABLE I. The ratio of total scattering in Ne to that in He, as determined by experiment and predicted by various levels of theory. The following predictions are shown: correlated CI form factors and incoherent-scattering factors, the exact-$A^2$ result, obtained by including the GOS corrections of Method A, and the full predictions of Methods A and B. (See the text for further details of the theoretical methods employed.) In the first column $K(\text{a.u.})=2\alpha\hbar\omega_0(\text{a.u.})\sin(\theta/2)$, where $\alpha$=the fine-structure constant.

| $K$ (a.u.) | $\hbar\omega_0$ (keV) | $\theta°$ | Experiment | CI | Exact $A^2$ | Method A | Method B |
|---|---|---|---|---|---|---|---|
| 0.90 | 4.39 | 45 | 24.4±0.4 | 23.13 | 23.18 | 24.42 | 24.15 |
| 1.23 | 6.00 | 45 | 22.5±0.3 | 21.48 | 21.55 | 22.37 | 22.17 |
| 1.67 | 4.39 | 90 | 20.2±0.3 | 18.68 | 18.84 | 20.08 | 19.96 |
| 1.67 | 8.12 | 45 | 19.2±0.2 | 18.68 | 18.77 | 19.27 | 19.02 |
| 1.85 | 9.00 | 45 | 17.7±0.2 | 17.39 | 17.48 | 17.92 | 17.68 |
| 2.28 | 6.00 | 90 | 15.5±0.2 | 14.37 | 14.55 | 15.29 | 15.35 |
| 3.08 | 8.12 | 90 | 10.5±0.1 | 9.96 | 10.11 | 10.47 | 10.46 |
| 3.08 | 15.00 | 45 | 10.0±0.1 | 9.96 | 9.99 | 10.18 | 10.11 |
| 3.41 | 9.00 | 90 | 9.1±0.1 | 8.74 | 8.87 | 9.21 | 9.15 |
| 5.69 | 15.00 | 90 | 5.8±0.1 | 5.77 | 5.82 | 5.90 | 5.89 |

analyses by three different observers using two different software packages. These differences for the Ne to He ratio did not exceed 0.3% for any of the data points.

## III. RESULTS

### A. Comparison with theoretical methods

Results for the ratio of total scattering from Ne to that from He are presented in Table I for the energies and angles that were investigated. Results are ordered in the table according to increasing momentum transfer $K$, and pairs of data corresponding to the same momentum transfer are grouped together for easy comparison. The experimental ratio (column 4) is compared with various theoretical results: results using the correlated configuration-interaction (CI) elastic form factors and inelastic incoherent-scattering factors of Wang *et al.* [3] (column 5), exact-$A^2$ results obtained by including the GOS corrections to the ISF of Method A (column 6), and the full predictions of Methods A and B (columns 7 and 8, respectively) which both include the elastic $\boldsymbol{p}\cdot\boldsymbol{A}$ contributions. (Inelastic $\boldsymbol{p}\cdot\boldsymbol{A}$ and relativistic contributions are not important in these situations.) Figure 2 compares the experimental results with the theoretical predictions of Methods A and B, as a function of energy, for each scattering angle. Note that in Fig. 2, each result is normalized to the experimental mean value of the case.

We see that the predictions of both Methods A and B are generally in agreement with the experimental results, although both methods appear to give higher values for the ratio than experiment at the highest energies. The general conclusion is that both the Methods A and B adequately agree with each other and with experiment. From Table I we see that the (simply momentum-transfer-dependent) predictions obtained using the best available form factors and incoherent-scattering factors (CI) are not sufficient. Going beyond this to exact-$A^2$ result, including GOS corrections, gives only a slight improvement. But going to the full result, including the $\boldsymbol{p}\cdot\boldsymbol{A}$ terms, using either Method A or B, leads to good agreement (columns 7 and 8). Therefore the most important contribution beyond using the best correlated form factors and incoherent-scattering factors is that of the anomalous elastic-scattering $\boldsymbol{p}\cdot\boldsymbol{A}$ terms. The ISF, while not corresponding to an exact evaluation of the inelastic $A^2$ term, appears to approximate it fairly well in obtaining total scattering in this low-energy and low-momentum transfer range where elastic scattering dominates.

In Table II we give correction factors characterizing the contributions of various effects in the total scattering cross section, again ordered according to increasing momentum transfer $K$, with pairs of data corresponding to the same momentum transfer grouped together. Results are given for helium and neon separately, and in each case the contribution of a given effect is expressed as a percentage of the (best) total scattering prediction for that element/energy/angle (this

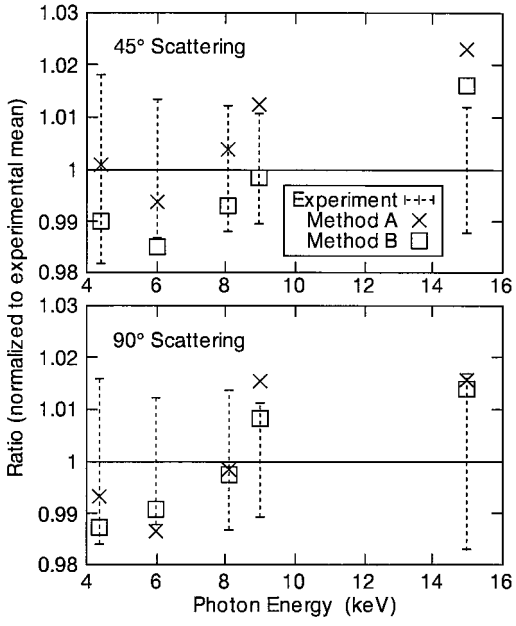


FIG. 2. Comparison of experimental results with theoretical predictions for the ratio of total scattering in Ne to that in He at 45° (top) and 90° (bottom). All results are normalized to the experimental mean values and the experimental error is indicated. See the text for details of the different theoretical methods employed.

TABLE II. Correction factors used in Methods A and B: In all cases the contribution of a given effect is expressed as a percentage of the total (elastic + inelastic) scattering cross section for the element/energy/angle being considered. In Method A, the correction $\delta_{\mathrm{GOS}}$ accounts for the difference between the ISF result and the exact-$A^2$ inelastic result. Similarly in Method B, $\delta_{\mathrm{IA}}$ accounts for the difference between the IA result and the exact-$A^2$ result for (inelastic) Compton scattering. Additionally, in Method B, one needs to add in the appropriate Raman-scattering cross section, and $\delta_{\mathrm{Raman}}$ expresses this contribution as a fraction of the total scattering. In both methods one also includes the contribution of the anomalous amplitudes, corresponding to $\delta_{\boldsymbol{p}\cdot\boldsymbol{A}}$.

| $K$ | $\hbar\omega_0$ | $\theta°$ | Helium | | | | Neon | | | |
|---|---|---|---|---|---|---|---|---|---|---|
| (a.u.) | (keV) | | $\delta_{\boldsymbol{p}\cdot\boldsymbol{A}}$ | $\delta_{\mathrm{GOS}}$ | $\delta_{\mathrm{IA}}$ | $\delta_{\mathrm{Raman}}$ | $\delta_{\boldsymbol{p}\cdot\boldsymbol{A}}$ | $\delta_{\mathrm{GOS}}$ | $\delta_{\mathrm{IA}}$ | $\delta_{\mathrm{Raman}}$ |
| 0.90 | 4.39 | 45 | 0.1% | −0.3% | −2.4% | 4.3% | 5.1% | −0.1% | −1.6% | 0.4% |
| 1.23 | 6.00 | 45 | 0.1% | −0.4% | −5.4% | 4.9% | 3.7% | −0.1% | −2.0% | 0.3% |
| 1.67 | 4.39 | 90 | 0.1% | −1.2% | −7.1% | 4.4% | 6.3% | −0.3% | −2.4% | 0.3% |
| 1.67 | 8.12 | 45 | 0.0% | −0.7% | −7.1% | 4.4% | 2.6% | −0.2% | −2.4% | 0.2% |
| 1.85 | 9.00 | 45 | 0.0% | −0.8% | −6.9% | 4.0% | 2.5% | −0.2% | −2.6% | 0.1% |
| 2.28 | 6.00 | 90 | 0.1% | −2.0% | −5.6% | 2.9% | 4.9% | −0.7% | −2.8% | 0.2% |
| 3.08 | 8.12 | 90 | 0.0% | −2.9% | −2.4% | 1.4% | 3.6% | −1.5% | −2.6% | 0.2% |
| 3.08 | 15.00 | 45 | 0.0% | −1.6% | −2.3% | 1.3% | 1.4% | −0.8% | −2.6% | 0.1% |
| 3.41 | 9.00 | 90 | 0.0% | −3.3% | −1.5% | 1.0% | 3.8% | −1.9% | −2.2% | 0.1% |
| 5.69 | 15.00 | 90 | 0.0% | −5.6% | 0.1% | 0.1% | 1.6% | −4.8% | −0.3% | 0.0% |

being the total cross section obtained by either Method A or B). In Method A the correction $\delta_{\mathrm{GOS}}$ accounts for the difference between the incoherent-scattering-factor result and the exact-$A^2$ inelastic result. Similarly in Method B, $\delta_{\mathrm{IA}}$ accounts for the difference between the impulse-approximation result and the exact-$A^2$ result for (inelastic) Compton scattering. Additionally in Method B one needs to add in the appropriate Raman-scattering cross section, and $\delta_{\mathrm{Raman}}$ expresses this contribution as a fraction of the total scattering. In both methods one also includes the contribution of the anomalous amplitudes, corresponding to $\delta_{\boldsymbol{p}\cdot\boldsymbol{A}}$.

What can we tell from Table II about the importance of additional effects beyond using the best (i.e., correlated) form factors and incoherent-scattering factors in our description of total scattering? Clearly one important effect is the contribution of the (elastic) $\boldsymbol{p}\cdot\boldsymbol{A}$ term for the case of neon, which is significant in all cases, though decreasing in magnitude with increasing energy. This contribution is insignificant for helium in all cases, since we are so far above the helium thresholds. The GOS corrections are often small (except at high energies) indicating that using the ISF to describe inelastic scattering is often fairly adequate in obtaining the total scattering in the $A^2$ approximation [using the form factor (FF) for the elastic scattering]. Note also that at high energies (where inelastic scattering is most important) the GOS corrections are similar for both He and Ne, so that the *ratio* of scattering in Ne to He, which we are measuring, is largely unchanged. If, however, in the spirit of Method B, one describes the total scattering in the $A^2$ approximation using IA to describe the inelastic piece, greater error is incurred (more so for He than for Ne). First of all, to do so entirely neglects Raman scattering, which can be significant, particularly for He. Also one is not even describing the Compton inelastic piece so well, as the corrections $\delta_{\mathrm{IA}}$ are themselves significant, particularly for He. Therefore one concludes that, in describing total scattering, using ISF alone for inelastic scattering is better than using IA alone.

### B. Comparisons at fixed momentum transfer

We now consider the two cases in which there are two measurements at the same value of the momentum transfer. The predictions for the two members of each pair are the same in the form-factor incoherent-scattering-factor approximation, hence any difference between the two ratios is a direct measurement of the sum of the GOS and $\boldsymbol{p}\cdot\boldsymbol{A}$ corrections. Looking back at Table I, we have grouped the pairs of measurements corresponding to the case of momentum transfer $K=1.67$, and likewise the pair with $K=3.08$. For each such pair of points we show the identical results of the form-factor incoherent-scattering-factor (CI) method, a slight difference between results using the exact-$A^2$ approximation (reflecting the GOS correction), and a more substantial difference between results using either of Methods A or B, showing that the influence of the $\boldsymbol{p}\cdot\boldsymbol{A}$ terms (included in both Methods A and B but not in the other predictions) is the dominant effect in the observed difference.

Looking now at Table II, focusing on these pairs of points of equal momentum transfer, we see significant and different corrections $\delta_{\boldsymbol{p}\cdot\boldsymbol{A}}$ (for neon) at the same momentum transfer. At a given momentum transfer the corrections are larger (here by a factor of $\approx 2$) for lower energy and larger angle, since the elastic anomalous $\boldsymbol{p}\cdot\boldsymbol{A}$ amplitudes are larger at lower energies and contribute more at larger angles where the form-factor contribution is dropping. We note that the exact $A^2$ contribution is not strictly a function of momentum transfer (though the elastic exact $A^2$ piece, the form factor, is). Thus additional differences arise from the beyond-incoherent-scattering-factor contributions—these are precisely the GOS corrections of Method A. Note that in Method B the situation is different. Here the correction to the IA result $\delta_{\mathrm{IA}}$ appears to be a function of momentum transfer only, but the IA result itself is not simply momentum-transfer dependent, but rather a function of energy and of angle.

TABLE III. Comparison of various levels of theory with experiment using the figure of merit $R$, defined in the text. Values of $R$ are given for the comparison of experiment with the following theoretical predictions: form factors and incoherent-scattering factors using local exchange (column 2), nonlocal HF form factors and incoherent-scattering factors (column 3), correlated CI form factors, and incoherent-scattering factors (column 4), the exact-$A^2$ result, obtained by including the GOS corrections of Method A (column 5), and the full predictions of Methods A and B (columns 6 and 7, respectively). The mean of the absolute value of the percentage experimental error is also given (column 8).

| Experiment | Local | HF | CI | Exact $A^2$ | Method A | Method B | Error |
|---|---|---|---|---|---|---|---|
| This paper | 5.3 | 2.3 | 2.2 | 3.5 | 0.9 | 0.9 | 1.3 |
| Ref. [2] | 2.0 | 5.2 | 4.3 | 1.7 | 1.1 | 1.2 | 1.7 |
| Ref. [1] | 3.6 | 1.1 | 0.4 | 0.4 | 0.7 | 0.6 | 0.5 |

### C. Comparisons with previous work

In order to survey the present and previous experiments in a succinct manner we utilize the figure of merit $R$, which is the mean of the absolute value of the percentage deviations of the experiment from a comparison theory:

$$R=\frac{1}{N}\sum_{i=1}^{N}\frac{\left|\frac{d\sigma}{d\Omega}_{\text{experiment}}(i)-\frac{d\sigma}{d\Omega}_{\text{theory}}(i)\right|}{\frac{d\sigma}{d\Omega}_{\text{experiment}}(i)}\times 100\%, \qquad (6)$$

where $N$ is the total number of data points collected in a particular experiment. Values of $R$ are shown in Table III for the present paper and for the studies reported in Refs. [1] and [2]. Values are given for the comparison of experiment with the following theoretical predictions: form factors and incoherent-scattering factors using local exchange (column 2), nonlocal Hartree-Fock (HF) form factors and incoherent scattering factors of Hubbell *et al.* [9] (column 3), correlated CI elastic form factors and incoherent scattering factors of Wang *et al.* [3] (column 4), exact-$A^2$ results including the GOS corrections of Method A (column 5), the full predictions of Method A including both the GOS corrections and the $\boldsymbol{p}\cdot\boldsymbol{A}$ contributions (column 6), and the predictions of Method B including the corrections to IA, Raman scattering, and the $\boldsymbol{p}\cdot\boldsymbol{A}$ contributions (column 7). The mean of the absolute value of the percentage experimental error is also given (column 8).

We note the sensitivity of all three experiments to the use of nonlocal versus local exchange. For the cases of this paper and that of Ref. [1], both measuring total scattering, a definite improvement is seen is going from using local exchange to using nonlocal exchange. In Ref. [2], however, both total scattering and ratios of elastic to inelastic scattering were measured, such that in averaging over all results one does better with a simple treatment using local exchange, instead of using nonlocal Hartree-Fock form factors and incoherent-scattering factors. We note that such fortuitous cancellations are not a general feature.

Assuming that one has adopted nonlocal exchange, it is clear that the present experiment is mainly sensitive to the $\boldsymbol{p}\cdot\boldsymbol{A}$ corrections, while the data in Ref. [2] are mainly sensitive to the GOS corrections, although some improvement is observed when the $\boldsymbol{p}\cdot\boldsymbol{A}$ corrections are added. In the case of the data reported in Ref. [1], the only major improvement beyond using nonlocal exchange has been achieved by the inclusion of corrections for electron correlation in the description of the target's electronic structure. This is a high-energy small-angle regime where accurate form factors and incoherent-scattering factors should perform well. Correlation (in contrast to exchange) did not play a major role in this experiment, or in Ref. [2].

## IV. CONCLUSIONS

Ratios of total scattering cross sections for gases can be determined with high accuracies, approaching $\pm 0.1\%$, by using third-generation synchrotron sources, accurate pressure gauges, and Be windows to cut down on air diffusion into the scattering cells. While previous experiments have demonstrated the need to include anomalous scattering contributions for small scattering angles, and the effects of nonlocal exchange and electron correlation, we have here demonstrated the need to include the anomalous scattering contributions at intermediate scattering angles (in particular by comparing pairs of measurements corresponding to different energies and angles but the same momentum transfer). We have also considered in detail the various theoretical approximations used to describe scattering, focusing on the corrections to the usual incoherent-scattering factor, and impulse approximations for inelastic-scattering. If one begins with the impulse approximation one needs to consider corrections to the impulse approximation and the contribution of Raman scattering in obtaining the inelastic-scattering cross section. In these cases the incoherent-scattering-factor approximation for inelastic scattering is generally adequate in obtaining the total scattering, while anomalous scattering factor corrections to form factors are needed for elastic scattering to achieve agreement with experiment.

## ACKNOWLEDGMENTS

The authors wish to thank the staff of BESSRC for their assistance in carrying out the experiment. This work is supported in part by the Chemical Sciences, Geosciences, and Biosciences Division of the Office of Basic Energy Sciences, Office of Science, U.S. Department of Energy, under Contract No. W-31-109-ENG-38 and in part by the National Science Foundation under Grants Nos. CHE-9705189 and PHY-9970293.

## APPENDIX A: DETAILS OF THE METHODS A AND B

### 1. Considerations common to both methods

As discussed in Sec. I, we first assume relativistic effects are small or negligible, allowing us to continue our discussion using the nonrelativistic form of the electron-photon interaction Eq. (1). Should one wish to include an estimate of relativistic effects, these could be gauged, for example, by a comparison of nonrelativistic [9] and relativistic [10] form factors (elastic case) and nonrelativistic [9] and relativistic [11] inelastic-scattering factors (inelastic case). Further we assume that estimates of $\boldsymbol{p}\cdot\boldsymbol{A}$ contributions are obtained from Ref. [12], neglecting inelastic $\boldsymbol{p}\cdot\boldsymbol{A}$ terms, which are insignificant for the cases under consideration (as is seen from a comparison of exact-$A^2$ and full dynamic $S$-matrix results). This leaves us with the $A^2$ term to consider for both the elastic and the inelastic cases.

The pure $A^2$ contribution to the angular dependent cross section can be written as

$$\left(\frac{d\sigma}{d\Omega}\right)_{\text{total}} = \left(\frac{d\sigma}{d\Omega}\right)_{\text{elastic}} + \left(\frac{d\sigma}{d\Omega}\right)_{\text{inelastic}} = \sigma_{\text{T}}\left\{ |F(K)|^2 + \sum_{n\neq 0}\left(\frac{\omega_n}{\omega_0}\right)\frac{K^2}{E}\frac{df(K,E)}{dE}\,\delta(\omega_0-\omega_n-E)\right\}, \quad \text{(A1)}$$

where $\sigma_{\text{T}}$ is the Thomson cross section, $\hbar\omega_n$ is the excitation energy of the final state, and the summation includes all excited discrete and continuum states consistent with energy conservation.

$$F(K) = \left\langle 0 \left| \sum_{i=1}^{N} e^{i\boldsymbol{K}\cdot\boldsymbol{r}_i} \right| 0 \right\rangle \quad \text{(A2)}$$

is the x-ray coherent scattering factor or form factor, and

$$\frac{df(K,E)}{dE} = \left(\frac{E}{K^2}\right)\sum_{p}\left|\left\langle p\left|\sum_{i=1}^{N} e^{i\boldsymbol{K}\cdot\boldsymbol{r}_i}\right|0\right\rangle\right|^2 \delta(E_p-E) \quad \text{(A3)}$$

is the GOS with $K$ the momentum transferred to the $N$ electron target by the photon, and $E$ is the photon energy transferred to the target (called the *energy loss*). The sum in Eq. (A3) is over all excited final states $|p\rangle$.

So, in the elastic case the $A^2$ term leads to the form factor Eq. (A2), which corresponds to the Fourier transform of the atomic wave function. Many tabulations of form factors are available, calculated using a wide variety of wave functions. Here (in both Methods A and B) we used the correlated form factors of Ref. [3], those being the highest quality believed to be available. We note that in form-factor approximation (i.e., neglecting $\boldsymbol{p}\cdot\boldsymbol{A}$ contributions) elastic scattering is simply a function of the momentum transfer only—deviations from this behavior are an indication of the influence of anomalous $\boldsymbol{p}\cdot\boldsymbol{A}$ contributions, as discussed in Sec. III B.

This leaves us only to obtain the inelastic $A^2$ scattering piece, i.e., the last term in Eq. (A1), which corresponds to an integration of the GOS Eq. (A3) over the allowed values for the energy loss $E$. Note that the possible final states in Eq. (A3) include both excited bound states (Raman scattering) and continuum states (Compton scattering). Since this term is complicated it is often dealt with by using approximations, leading, for example, to the ISF or the IA. We now describe the implementations of Methods A and B, which (approximately) recover the exact-$A^2$ inelastic results starting from the ISF and IA, respectively.

### 2. Implementation of Method A

If the energy-conservation restriction is ignored $\omega_n/\omega_0$ is approximated by unity, and $K$ is replaced by the momentum transfer for elastic scattering, $K_{\text{elastic}}(\text{a.u.}) = 2\alpha\hbar\omega_0(\text{a.u.})\sin(\theta/2)$, then the sum in Eq. (A1) can be carried out exactly [13] with the result

$$K_{\text{elastic}}^2\sum_{n\neq 0}\frac{1}{E}\frac{df(K_{\text{elastic}},E)}{dE}\,\delta(\omega_0-\omega_n-E) = S(K_{\text{elastic}}), \quad \text{(A4)}$$

where

$$S(K_{\text{elastic}}) = N + \left\langle 0\left|\sum_{i\neq j}^{N}\exp(i\boldsymbol{K}_{\text{elastic}}\cdot\boldsymbol{r}_{ij})\right|0\right\rangle - |F(K_{\text{elastic}})|^2 \quad \text{(A5)}$$

is the x-ray incoherent-scattering factor. Wang *et al.* [3] report values of $S(K_{\text{elastic}})$ for He and Ne, which include 99 and 80% of the correlation, respectively, while Ref. [5] contains values of $S(K_{\text{elastic}})$ for Ne with 95.7% of the correlation included. The best estimate for the exact theoretical value for $S(K_{\text{elastic}})$ was obtained by linear extrapolation of the results given in Refs. [3] and [5] as a function of the percentage of correlation.

It only remains to estimate the difference between Eq. (A4) and the inelastic sum in Eq. (A1) in order to arrive at an accurate estimate for the $A^2$ contribution to the total inelastic x-ray scattering. The details of the approximate calculation of the difference, called the GOS correction, are given in Refs. [15] and [7]. For an accuracy commensurate with the experimental uncertainties of this paper, the GOS corrections can be included by replacing $S(K_{\text{elastic}})$ by

$$S(K_{\text{elastic}}) - 2N\left(\frac{\hbar\omega_0}{mc^2}\right)\sin^2\left(\frac{\theta}{2}\right)\left\{1-\left(\frac{\hbar\omega_0}{mc^2}\right)\left[3\sin^2\left(\frac{\theta}{2}\right)+\frac{1}{2}\right] + \left(\frac{\hbar\omega_0}{mc^2}\right)^2\sin^2\left(\frac{\theta}{2}\right)\left[4\sin^2\left(\frac{\theta}{2}\right)+\frac{9}{4}\right]\right\}. \quad \text{(A6)}$$

Therefore the finite second term in Eq. (A6) gives rise to the GOS correction.

### 3. Implementation of Method B

In Compton scattering the impulse approximation is often used. We obtain the difference between the IA result and the exact $A^2$ Compton results by assuming linear independence of a number of effects (correlation, nonlocality, $A^2$ corrections to impulse), allowing us to use perturbative estimates to construct the full result. Since local uncorrelated estimates of

the $A^2$ correction to IA are available, we can first include these, then include the other effects, using the data available, as described in Ref. [6]. How one obtains a corresponding ''better'' prediction for the scattering cross section from a ''simple'' result, using the composite method, can be symbolically represented as

$$\left(\frac{d\sigma}{d\Omega}\right)_{\text{better}} = \left(\frac{d\sigma}{d\Omega}\right)_{\text{simple}} \left(1+\sum_i \delta_i\right), \tag{A7}$$

where the summation is over all corrections $\delta_i$ associated with independent perturbative effects not included in the ''simple'' calculation.

One should also then include estimates of the inelastic Raman-scattering. Note that at higher energies, as in Ref. [2], this piece is small and can also be included perturbatively, or even neglected. However in the present case it is important, particularly for He. Hydrogenic results indicate that the $\boldsymbol{p}\cdot\boldsymbol{A}$ contribution to the Raman scattering cross section is insignificant in this case, with the high-momentum-transfer contribution being given by the $A^2$ term. Here we directly calculate the Raman $A^2$ result using local exchange, and add perturbative corrections according to be method described in Ref. [6], based on results for the generalized oscillator strength for excitation to excited bound states (see, e.g., Ref. [14]). One can also sum Raman and Compton cross sections evaluated using local exchange and then apply nonlocal-exchange and correlation correction to this sum, based on ISF results—which is consistent since the ISF is an approximation to the sum of Compton and Raman (total inelastic) scattering.

## APPENDIX B: ION AND DETECTOR RESPONSE

In order to explore the effects of window absorption and detector response on the measured cross section we use the following model for the doubly differential cross section

$$\frac{d^2\sigma(\varepsilon)}{dEd\Omega} = \left(\frac{d\sigma}{d\Omega}\right)_{\text{elastic}} \delta(\varepsilon) + \left(\frac{d\sigma}{d\Omega}\right)_{\text{inelastic}} \frac{1}{\sqrt{2\pi}\sigma_C} \times \exp[-(\varepsilon - E_C)^2/2\sigma_C^2], \tag{B1}$$

where $\sigma_C$ and $E_C$ characterize the width and the energy loss for the Compton peak. The detector response is given by

$$R(\sigma_R,\alpha,\varepsilon) = S(\sigma_R,\varepsilon)\xi(\alpha,\varepsilon), \tag{B2}$$

where the detector efficiency, $\xi$, is modeled as

$$\xi(\alpha,\varepsilon) = 1+\alpha\varepsilon, \tag{B3}$$

with $\alpha>0$ and

$$S(\sigma_R,\varepsilon) = \frac{1}{\sqrt{2\pi}\sigma_R}\exp[-\varepsilon^2/2\sigma_R^2] \tag{B4}$$

is an approximation to the delta function response for the detector, which has an energy resolution of $\pm\sigma_R$. The window transmission is modeled as

$$T_{w3}(\varepsilon) = 1-\beta\varepsilon, \tag{B5}$$

with $\beta>0$. The model choices are dictated by the fact that the corrections are expected to be small so that a crude model should suffice for the purpose of estimating the corrections. The convolution of the response with the doubly differential cross section can be evaluated as

$$\begin{aligned}\int_{-\infty}^{\infty} d\varepsilon R(\sigma_R,\alpha,E-\varepsilon)\left(\frac{d^2\sigma_{1,2}(\varepsilon)}{dEd\Omega}\right) &= \left(\frac{d\sigma}{d\Omega}\right)_{\text{elastic}} R(\sigma_R,\alpha,E) + \left(\frac{d\sigma}{d\Omega}\right)_{\text{inelastic}} \\ &\times\left\{R\left[\sigma_f,\alpha\left(\frac{\sigma_R}{\sigma_f}\right)^2,E-E_C\right]\left(\frac{\alpha\sigma_R^2\sigma_C^2}{\sigma_f^2}\right)\right. \\ &\times[S(\sigma_R,E-\hbar\omega_0+\Delta)S(\sigma_C,E_C-\hbar\omega_0+\Delta) \\ &\left.-S(\sigma_R,E+2\hbar\omega_0)S(\sigma_C,E_C+2\hbar\omega_0)]\right\},\end{aligned} \tag{B6}$$

where $\sigma_f=\sqrt{\sigma_R^2+\sigma_C^2}$, the limits of the integration approximate the upper and lower threshold settings of the pulse height analyzer, and the lower limit $\Delta$, is usually no larger than a few hundred eV or $<(1/40)\hbar\omega_0$. Note that the last two terms in Eq. (B6) make their largest contribution only when $E\approx\hbar\omega_0$ or $-2\hbar\omega_0$.

Equation (B6) times the window transmission can be integrated over the observed energy-loss spectrum with the approximate result

$$\begin{aligned}\left(\frac{d\sigma_{1,2}^{\text{exp}}(\theta,\hbar\omega_0)}{d\Omega}\right) &= \int_{E_{\min}}^{E_{\max}} dE T_{w3}(E)\int_{-\infty}^{\infty} d\varepsilon R(E-\varepsilon)\left(\frac{d^2\sigma_{1,2}(\varepsilon)}{dEd\Omega}\right) \\ &\simeq \left(\frac{d\sigma}{d\Omega}\right)_{\text{elastic}}\{1+(\beta-\alpha)\sigma_R^2[S(\sigma_R,E_{\max})-S(\sigma_R,E_{\min})]\} + \left(\frac{d\sigma}{d\Omega}\right)_{\text{inelastic}}\left\{(1-\beta E_C)+\frac{(\beta\sigma_f^4-\alpha\sigma_R^4)}{\sigma_f^2}\right. \\ &\times[S(\sigma_f,E_{\max}-E_C)-S(\sigma_f,E_{\min}-E_C)] + \left(\frac{\alpha\sigma_R^2\sigma_C^2}{\sigma_f^2}\right)[S(\sigma_C,E_{\max}-E_C)-S(\sigma_C,E_{\min}-E_C)]\left.\right\},\end{aligned} \tag{B7}$$

where $E_{\min}$ and $E_{\max}$ are the limits for summing up counts in the recorded spectrum and are usually chosen as $E_{\max}=3$–4 keV and $E_{\min}\simeq-\hbar\omega_0$. Since this interval contains the entire spectrum the integration limits can be taken from $-\infty$ to $\infty$ as before when dealing with the pure Gaussian terms. For the exponential terms (i.e., terms involving integrals of the type $\int dE\, E\exp[-E^2/2\sigma^2]$) which contain all the corrections, except for the term $(d\sigma/d\Omega)_{\text{inelastic}}(1-\beta E_C)$, the integrals were carried out with the exact limits in order to assess the value of their contribution. Equation (B7) was evaluated numerically for all the observations. The radiation passed through a 125-$\mu$m Kapton window and a 7.5-$\mu$m Be window at 45° and the same thickness Kapton window with a 25-$\mu$m Be window at 90°. Only the window transmission produced an appreciable correction as the shape factors, $S(\alpha,E)$, were all found to be extremely small. It was discovered that the decrease in the slope $\beta$ with increasing incident x-ray energy outweighed the increase in $E_C$ so that the largest corrections occurred at the lowest incident energy. A correction $\Lambda$ defined as

$$\Lambda=\left(\frac{[F(K)^2+S(K)(1-\beta E_C)]_{\text{He}}}{[F(K)^2+S(K)]_{\text{He}}}\right)\times\left(\frac{[F(K)^2+S(K)]_{\text{Ne}}}{[F(K)^2+S(K)(1-\beta E_C)]_{\text{Ne}}}\right) \tag{B8}$$

was multiplied by each experimental ratio to obtain the final result for the experimental ratios. In Eq. (B8) $\beta$ was obtained by fitting the transmission through the Kapton and Be windows to a straight line over an energy range beyond the position of the elastic line that varied from 200 eV at 4.393 keV to 900 eV at 15 keV. The parameter $E_C$ is the energy-loss position of the center of the Compton peak. The correction was largest for 90° and 4.393 keV, where it amounted to a 0.7% decrease in the ratio.

## APPENDIX C: DETAILS OF CORRECTIONS TO EXPERIMENTAL RATIOS

The ratio of the two detected signals with He in cell 1 and Ne in cell 2, using the notations introduced in Eqs. (2) and (3), is then

$$\frac{I_{\text{Ne}}(\theta,\hbar\omega_0)}{I_{\text{He}}(\theta,\hbar\omega_0)}=T_{w2}^2\exp[-(l_3-l_2)n_{\text{He}}\sigma_{\text{He}}-(l_1+l_2)n_{\text{Ne}}\sigma_{\text{Ne}}]\left(\frac{n_{\text{Ne}}}{n_{\text{He}}}\right)\times\left[\left(\frac{d\sigma_{\text{Ne}}^{\text{exp}}(\theta,\hbar\omega_0)}{d\Omega}\right)\Big/\left(\frac{d\sigma_{\text{He}}^{\text{exp}}(\theta,\hbar\omega_0)}{d\Omega}\right)\right], \tag{C1}$$

where we have assumed that the two detectors have the same response. For the runs in which both cells are filled with He to a number density $n'_{\text{He}}$, the ratio reduces to

$$\frac{I_{\text{He}-2}(\theta,\hbar\omega_0)}{I_{\text{He}-1}(\theta,\hbar\omega_0)}=T_{w2}^2\exp[-(l_3+l_1)n'_{\text{He}}\sigma_{\text{He}}], \tag{C2}$$

which can be used to eliminate the window scattering by dividing it in to the previous result. We treat the exponential terms as corrections calculated from tabulated transmission factors [16] for 1 cm of gas at a pressure $P_0$, assuming that the gases are ideal and at the same temperature, so that our final result for the desired ratio can be written in terms of experimentally measured quantities as

$$\left[\left(\frac{d\sigma_{\text{Ne}}^{\text{exp}}(\theta,\hbar\omega_0)}{d\Omega}\right)\Big/\left(\frac{d\sigma_{\text{He}}^{\text{exp}}(\theta,\hbar\omega_0)}{d\Omega}\right)\right]=T_{\text{He}}(1\text{ cm},P_0)^{[(l_3-l_2)(P_{\text{He}}/P_0)-(l_1+l_3)(P'_{\text{He}}/P_0)]}\times T_{\text{Ne}}(1\text{ cm},P'_0)^{(l_1+l_2)(P_{\text{Ne}}/P'_0)}\times\left(\frac{P_{\text{He}}}{P_{\text{Ne}}}\right)\frac{[I_{\text{Ne}}(\theta,\hbar\omega_0)/I_{\text{He}}(\theta,\hbar\omega_0)]}{[I_{\text{He}-2}(\theta,\hbar\omega_0)/I_{\text{He}-1}(\theta,\hbar\omega_0)]}, \tag{C3}$$

where all distances are measured in centimeters and $T_{\text{He}}(1\text{ cm},P_0)$ and $T_{\text{Ne}}(1\text{ cm},P'_0)$ are the transmissions through 1 cm of He and Ne gas with $P_0=760$ Torr and $P'_0=80$ Torr. Equation (C3) will serve as the basis for analyzing the experimental data presented here. The transmission corrections varied from $17\%\pm0.6\%$ to $0.5\%\pm0.01\%$ for the 4.393 to 15.0 keV data sets, respectively.

As an interesting aside, if Ne is placed in cell 1 and He in cell 2 at the same pressures that were used in Eq. (C1), and the results are divided into the previous result, the gas absorption of the beam passing through the cell can be eliminated with the result for the cross section ratio

$$\left[\left(\frac{d\sigma_{\text{Ne}}^{\text{exp}}(\theta,\hbar\omega_0)}{d\Omega}\right)\Big/\left(\frac{d\sigma_{\text{He}}^{\text{exp}}(\theta,\hbar\omega_0)}{d\Omega}\right)\right]=\left(\frac{P_{\text{He}}}{P_{\text{Ne}}}\right)\sqrt{\frac{[I_{\text{Ne}-2}(\theta,\hbar\omega_0)/I_{\text{He}-1}(\theta,\hbar\omega_0)]}{[I_{\text{He}-2}(\theta,\hbar\omega_0)/I_{\text{Ne}-1}(\theta,\hbar\omega_0)]}}. \tag{C4}$$

This option was not selected for the present paper because of practical difficulties in matching the pressures accurately.

[1] D. R. Chipman and L. D. Jennings, Phys. Rev. **132**, 728 (1963).
[2] M. Jung, R. W. Dunford, D. S. Gemmell, E. P. Kanter, B. Krässig, T. W. LeBrun, S. H. Southworth, L. Young, J. P. J. Carney, L. LaJohn, R. H. Pratt, and P. M. Bergstrom, Jr., Phys. Rev. Lett. **81**, 1596 (1998).
[3] J. Wang, R. O. Esquivel, V. H. Smith, Jr., and C. F. Bunge, Phys. Rev. A **51**, 3812 (1995).
[4] H. Meyer, T. Müller, and A. Schweig, Acta Crystallogr., Sect. A: Found. Crystallogr. **51**, 171 (1995).
[5] H. Meyer, T. Müller, and A. Schweig, Chem. Phys. **191**, 213 (1995).
[6] J. P. J. Carney and R. H. Pratt, Phys. Rev. A **62**, 012705 (2000).
[7] R. A. Bonham, J. Mol. Struct.: THEOCHEM **527**, 103 (2000).
[8] B. Zhou, L. Kissel, and R. H. Pratt, Phys. Rev. A **45**, 6906 (1992).
[9] J. H. Hubbell, Wm. J. Veigele, E. A. Briggs, R. T. Brown, D. T. Cromer, and R. J. Howerton, J. Phys. Chem. Ref. Data **4**, 471 (1975).
[10] J. H. Hubbell and I. Øverbø, J. Phys. Chem. Ref. Data **8**, 69 (1979).
[11] S. Kahane, At. Data Nucl. Data Tables **68**, 323 (1998).
[12] Results within the MFF+ASF approximation for Rayleigh scattering, giving the real and imaginary parts of the $\boldsymbol{A}\cdot\boldsymbol{p}$ correction, were obtained from http://www-phys.llnl.gov/Research/scattering/. See also L. Kissel, B. Zhou, S. C. Roy, S. K. Sen Gupta, and R. H. Pratt, Acta Crystallogr., Sect. A: Found. Crystallogr. **51**, 271 (1995).
[13] M. Inokuti, Rev. Mod. Phys. **43**, 1460 (1965).
[14] K. L. Bell, D. J. Kennedy, and A. E. Kingston, J. Phys. B **1**, 204 (1968).
[15] R. A. Bonham, Phys. Rev. A **23**, 2950 (1981).
[16] The transmission factors were obtained from absorption cross section values available at http://www-cxro.lbl.gov/optical_constants. See also B. L. Henke, E. M. Gullikson, and J. C. Davis, At. Data Nucl. Data Tables **54**, 181 (1993).